EasyChair Preprint

№ 5215

Dynamic Surface Control of the Axial-Flux Permanent Magnet Motor with Speed Sensorless Algorithm

Manh Tung Ngo, Quang Dang Pham, Huy Phuong Nguyen and Tung Lam Nguyen

March 24, 2021

Dynamic Surface Control of the Axial-Flux Permanent Magnet Motor with Speed Sensorless Algorithm

Ngo Manh Tung[1,2], Pham Quang Dang[1], Nguyen Huy Phuong[1], Nguyen Tung Lam[1][0000-0003-4108-8275]

[1] Hanoi University of Science and Technology, 1 Dai Co Viet Road, Viet Nam
[2] Hanoi University of Industry, No.298, Cau Dien Street, Bac Tu Liem District, Viet Nam
lam.nguyentung@hust.edu.vn

Abstract. The permanent synchronous motor drive system incorporates magnetic bearings to perform speed control and balance rotor control between the two stators. The paper designed a system to perform adjusting motor speed sensorless based on measured current and voltage components. The electromotive force (back-EMF) generated in the stator is estimated by a High-Gain observer. The angular position and velocity rotor is calculated through the α-β components of the back-EMF. The motor drive is built in a vector control structure based on the rotor flux. In which based on the Lyapunov stabilization function, the dynamic surface control method is used to calculate the axial position and speed controller of the motor. Simulation results show that the proposed controller and observer are fully capable of meeting the system control requirements.

Keywords: Magnetic self-bearing motor, Back-EMF, High-gain observer, dynamic surface control.

1 Introduce

In recent years, the motor with integrated magnetic bearing has been increasingly studied and applied due to its advantages compared to traditional ball bearing [1]. The motor has the magnitude of the air gap between the stator and the rotor is constantly varying, affecting the motor parameters and increasing the nonlinearity of the target. To deal with this problem, the control process needs to separate the channel between the torque generating the rotation and the force acting the axial position. Hence, based on the principle of control based on the rotor flux, the current i_d controls the axial force, while the radial current i_q controls the torque [2]. Dynamic surface control method is used to design the axial position controller and the motor speed control. This is a technique applied to nonlinear system objects, applied to grip control and stability for the system [3]–[5]. Therefore, this method is very suitable for the subject in the paper. The Dynamic Surface Control (DSC) technique features Backstepping and sliding multi-surface control (MSS) [6]. However, it has added a first order filter to overcome the problem of explosion of term.

During the control process, the control loops need to convert the coordinate system [7]. This leads to a need for accurate angular position information of the rotor by sensors

that measure the rotational angle. This increases costs, increases size, affects the mechanical strength and maintains equipment maintenance. Therefore, methods of replacing speed sensors with calculation techniques are studied and published more and more. In the published works on non-measuring rotation speed control for synchronous motors, two approaches for estimating the angular position and rotor speed can be given [8], [9].

This article presents a High-Gain observation based on the back-EMF electrodynamic reactivity estimation, it has the advantage that the rule of observation is simple, easy to design, and there is no project using HG observers for magnetic motors. Although [10] uses a similar observational structure, the hydraulic system applies. The paper proposes a drive system using a vector control structure, in which the HG observer estimates the back-EMF value from the stator current and the reference voltage value, thereby calculating the Rotor angle position and rotation speed.

The feasibility of the proposed methods is demonstrated through simulation of the control system without speed sensor on the software. Simulation results show that both position response and speed response follow the set trajectory in fast time. The system is also stable to the coupling effects of the two control loops.

2 Mathematical Model

The permanent magnet synchronous motor incorporating the axial magnetic bearing has the structure shown in Fig 1. The motor structure consists of a rotor and two stators [1]. The torque T that rotates the rotor is the sum of the two component moments and the F axial force that stops the rotor from moving in the z direction is calculated by the difference of the two axial forces. To design the control system, the mathematical model of the motor is shown on the dq rotating coordinate or $\alpha\beta$ static coordinate system. For L'_{sd0} and L'_{sq0}: the d- axis and q- axis inductance per gap unit; L_{sl}: leakage inductance; $g = g0 \pm z$: clearance between stator and rotor; g_0: clearance at equilibrium position; z: displacement. Voltage vector equation of a stator on the $\alpha\beta$ coordinate system is given as:

$$U_s = i_s R_s + L_s di_s / dt + E_s \tag{1}$$

The inductance is presented as [1], [11]:

$$L_{sd} = 3L'_{sd0} / 2g + L_{sl}; L_{sq} = 3L'_{sq0} / 2g + L_{sl} \tag{2}$$

Where i_s the stator current vector, U_s is the stator voltage vector. E_s is a sine function and is expressed as components on the $\alpha\beta$ coordinate system as follows:

$$E_{s\alpha} = -|\lambda_m| \omega_e \sin\theta_e; E_{s\beta} = |\lambda_m| \omega_e \cos\theta_e \tag{3}$$

With ω_e is the rotor speed, θ_e is the position of the rotor flux vector. From (1) we have:

$$\begin{cases} di_{s\alpha} / dt = -R_s i_{s\alpha} / L_{sd} + u_{s\alpha} / L_{sd} - E_{s\alpha} / L_{sd} \\ di_{s\beta} / dt = -R_s i_{s\beta} / L_{sq} + u_{s\beta} / L_{sq} - E_{s\beta} / L_{sq} \end{cases} \tag{4}$$

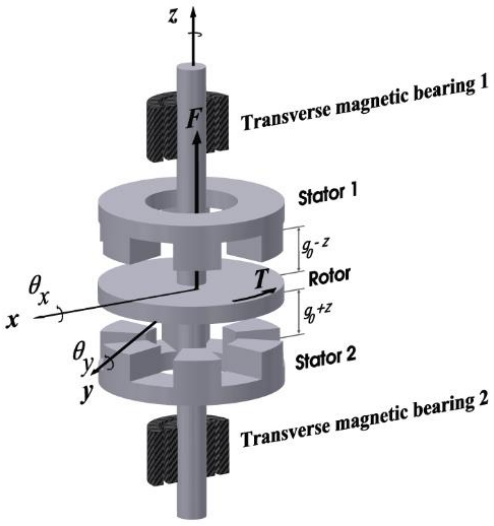

Fig. 1. The structure of the motor

We have the equation for calculating the total torque and total axial force as follows [11], [12]:

$$F = 4K_{Fd} i_f i_d ; T = 2K_T i_q \quad (5)$$

3 Design dynamic surface controls

The motor's rotation equation can be written as follows:

$$T - T_L = J.d\omega / dt \text{ or can be written as } \dot{\omega} = (T - T_L)/J \quad (6)$$

According to (6) we have: $\dot{\omega} = i_q.2K_T / J - T_L / J = M.i_q - N$ (7)

The definition of a sliding surface is: $z_1 = \omega - \omega_d$ (8)

The derivatice of z_1 is: $\dot{z}_1 = \dot{\omega} - \dot{\omega}_d = Mi_q - N - \dot{\omega}_d$ (9)

According to DSC, virtual control signal: $i_q = -c_\omega z_1 / M + (N + \omega_d)/M$ (10)

Choose a factor $c_\omega > 0$. The signal controls i_q through the filter which is the first-order filter to obtain the reference signal i_{qref}: $\dot{i}_{qref} = (i_q - i_{qref})/\tau_\omega$ (11)

Choose time constant $\tau_\omega > 0$. Set: $\tilde{i}_q = i_{qref} - i_q$ (12)

Suppose a Lyapunov candidate function is as follows: $V = z_1^2/2 + \tilde{i}_q^{\,2}/2$ (13)

In order for the speed loop to be controlled asymptotically, then the derivative of V:

$$\dot{V} = z_1 \dot{z}_1 + \tilde{i}_q \dot{\tilde{i}}_q \le 0 \quad (14)$$

According to (14), the time constant satisfies the following inequality:

$$\tau_\omega \le \varepsilon_\omega / B^2 \quad (15)$$

where $B > 0$ is a maximum constant that $\left|\dot{i}_q\right| \le B$.

According to (5): $\ddot{z} = (F - F_L)/m = 4K_{Fd} i_f i_d / m - F/m = P.i_d - Q$ (16)

Definition of sliding surface: $S = \dot{z} + \lambda z$ (choose factor $\lambda > 0$) (17)

Calculations similar to the speed controller, virtual control signal are defined [10]:

$$i_d = Q/P - \lambda \dot{z}/P - c_z.sat(S); \dot{i}_{dref} = (i_d - i_{dref})/\tau_z \quad (18)$$

Choose $c_z > 0$, $\tau_z > 0$ and the time constant should be satisfied: $\tau_z \le \varepsilon_z / A^2$ (19)

Where A is a maximum constant that $\left|\dot{i}_d\right| \le A$. The position control loop will stabilize after a finite time with z approaching sliding surface S.

4 High-gain observer design

From (3) and (4) we have:

$$\begin{aligned} e_{s\alpha} &= -\left|\lambda_m\right| \omega_e \sin\theta_e = -L_{s\alpha} \frac{di_{s\alpha}}{dt} - R_s i_{s\alpha} + u_{s\alpha} \doteq h_\alpha \\ e_{s\beta} &= \left|\lambda_m\right| \omega_e \cos\theta_e = -L_{s\beta} \frac{di_{s\beta}}{dt} - R_s i_{s\beta} + u_{s\beta} \doteq h_\beta \end{aligned} \quad (20)$$

The derivative property equation for $\hat{e}_{s\alpha}$ and $\hat{e}_{s\beta}$ according to the HGO set is written as follows [10], [13], with $1/\varepsilon_\alpha$ and $1/\varepsilon_\beta$ are the coefficients of HGO:

$$\begin{aligned} \dot{\hat{e}}_{s\alpha} &= (-L_{s\alpha}\dot{i}_{s\alpha} - R_s i_{s\alpha} + u_{s\alpha} - \hat{e}_{s\alpha})/\varepsilon_\alpha = -\hat{e}_{s\alpha}/\varepsilon_\alpha + h_\alpha/\varepsilon_\alpha \\ \dot{\hat{e}}_{s\beta} &= (-L_{s\beta}\dot{i}_{s\beta} - R_s i_{s\beta} + u_{s\beta} - \hat{e}_{s\beta})/\varepsilon_\beta = -\hat{e}_{s\beta}/\varepsilon_\beta + h_\beta/\varepsilon_\beta \end{aligned} \quad (21)$$

The definition of the error between the actual and the estimated value is as follows:

$$\tilde{e}_{s\alpha} = e_{s\alpha} - \hat{e}_{s\alpha}; \tilde{e}_{s\beta} = e_{s\beta} - \hat{e}_{s\beta} \quad (22)$$

According to [13], we have the following values satisfying the inequality:

$$\left|\tilde{e}_{s\alpha}\right| \le e^{(-1/\varepsilon_\alpha)t} \left|\tilde{e}_{s\alpha}(0)\right| + \varepsilon_\alpha.\rho_\alpha(t); \left|\tilde{e}_{s\beta}\right| \le e^{(-1/\varepsilon_\beta)t} \left|\tilde{e}_{s\beta}(0)\right| + \varepsilon_\beta.\rho_\beta(t) \quad (23)$$

From (20), the values $e_{s\alpha}$ and $e_{s\beta}$ are harmonic functions, so the coefficients $\dot{h}_{\alpha_{\max}}$ and $\dot{h}_{\beta_{\max}}$ exist such that: $\left|\dot{h}_\alpha\right| \le \dot{h}_{\alpha_{\max}}$ and $\left|\dot{h}_\beta\right| \le \dot{h}_{\beta_{\max}}$ (24)

Thus, the smaller the coefficients ε_α and ε_β, the smaller $\left|\tilde{e}_{s\alpha}\right|$ and $\left|\tilde{e}_{s\beta}\right|$ are blocked by the smaller bounding regions $\left|\tilde{e}_{s\alpha}(\infty)\right|$ and $\left|\tilde{e}_{s\beta}(\infty)\right|$. Then, the smaller the value ε_α and ε_β, the faster the rate of convergence of the estimated value follows the real values $e_{s\alpha}$và $e_{s\beta}$ of the back-EMF. From the output signal of High-gain observer, the values of the angular position and rotor speed are calculated as follows:

$$\hat{\theta}_e = \arctan(-\hat{E}_{s\alpha}/\hat{E}_{s\beta}) \quad (25)$$

$$\hat{\omega}_e = \sqrt{\hat{E}_{s\alpha}^2 + \hat{E}_{s\beta}^2} / \lambda_m (a) \text{ or: } \hat{\omega}_e = d\hat{\theta} / dt (b) \qquad (26)$$

Note that if the speed is calculated according to (35a), the value of the speed depends on the linkage flux λ_m, which is influenced by the ambient temperature. If used according to (35b), the speed is more reliable, especially in the medium and high-speed range, but is affected by process noise.

5 Simulation and result

The parameters of the motor include: phase resistance is 2.6 Ω; the air gap between the stator and the rotor is 1 mm; the rotor mass is 0.28kg; the moment of inertia is 10.6x10-6 kgm2; the amplitude of the flux flux generated by the permanent magnet is λ_m = 0.022 Wb.

When the set speed is 4500 rpm, at the moment of 0.65 s the load torque affects the system. Fig. 3 shows that the estimation speed is very fast with real speed value and the error is negligible.

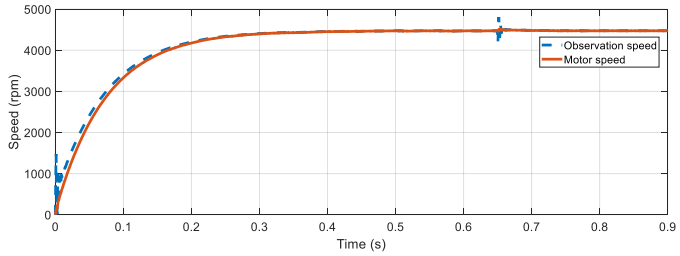

Fig. 3. Speed response when set value is 4500 rpm under the influence of load torque

Fig. 4 shows the response of the two current i_d and i_q, where the i_q current at the beginning has a large value to accelerate the motor to quickly reach the set value, then the value drops very small at the end of the transition mode. Fig.5 shows that when the load is applied, the back-EMF component on of the observer adheres to the back-EMF component of the motor very fast and few errors. Thus, in this case the HG observer estimates that the components $e_{s\alpha}$ and $e_{s\beta}$ have a sinusoidal form, with the same amplitude and following the observed value.

When changing the speed setting value from 2500 rpm-3500 rpm-1500 rpm in Fig. 7. Estimated speed is still capable of adhering to the real speed. The components e_s at the output of the HGO continue to be the same sinusoidal form and follow the motor Back-EMF. Changing the speed setting value does not change the estimation time of the monitor.

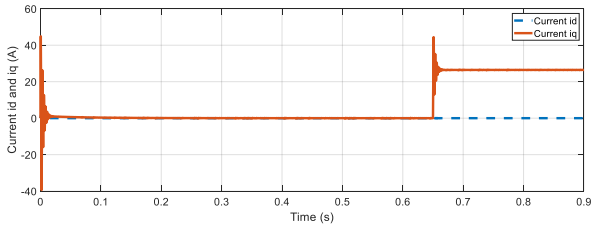

Fig. 4. Current response i_d and i_q

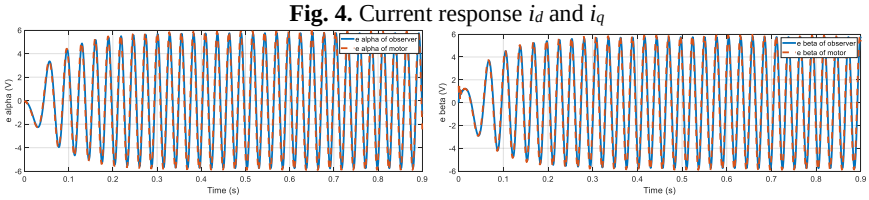

Fig. 5. $e_{s\alpha}$ and $e_{s\beta}$ component of the motor and $e_{s\alpha}$ and $e_{s\beta}$ set of the observation

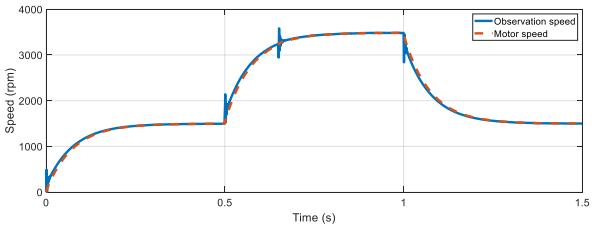

Fig. 6. Speed response

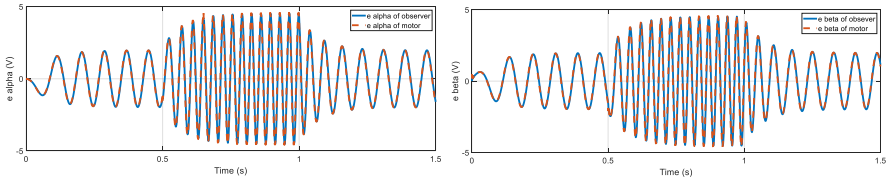

a) Response of e_alpha b) Response e_beta

Fig. 7. Back-EMF components on α-β trục axis when speed setting value is changed

6 Simulation and result

The paper presented the control system without measuring the rotation speed for synchronous motor with integrated magnetic bearing, calculating the dynamic surface controllers and designing the HGO unit in the system. By taking the input signal to the observer, the reference voltage and stator current perform an estimate of the back-EMF electromotive force as the basis for calculating the position and rotor speed. The system works stably at medium speed range upwards, in which the interaction between axial position control and speed control has also been limited. However, the peak phenomenon caused by the visual disturbance affects the quality of the output speed.

References

1. Q. Nguyen and S. Ueno, “Salient pole permanent magnet axial-gap self-bearing motor,” no. Im, 2009, doi: 10.5772/intechopen.83966.
2. R. He and Q. Han, “Dynamics and Stability of Permanent-Magnet Synchronous Motor,” Math. Probl. Eng., vol. 2017, 2017, doi: 10.1155/2017/4923987.
3. B. S. J. K. Hedrick, Dynamic Surface Control of Uncertain Nonlinear Systems. .
4. Y. H. Lan and Lei-Zhou, “Backstepping Control with Disturbance Observer for Permanent Magnet Synchronous Motor,” J. Control Sci. Eng., vol. 2018, 2018, doi: 10.1155/2018/4938389.
5. Z. J. Yang, T. Nagai, S. Kanae, and K. Wada, DYnamic surface control approach to adaptive robust control of nonlinear systems in semi-strict feedback form, vol. 16, no. 1. IFAC, 2005.
6. T. D. Nguyen, K. J. Tseng, S. Zhang, and H. T. Nguyen, “A novel axial flux permanent-magnet machine for flywheel energy storage system: Design and analysis,” IEEE Trans. Ind. Electron., vol. 58, no. 9, pp. 3784–3794, 2011, doi: 10.1109/TIE.2010.2089939.
7. N. P. Quang and J.-A. Dittrich, Power Systems Vector Control of Three-Phase AC Machines. .
8. Q. D. Nguyen and S. Ueno, “Sensorless speed control of inset type axial gap self-bearing motor using extended EMF,” 2010 Int. Power Electron. Conf. - ECCE Asia -, IPEC 2010, pp. 2260–2264, 2010, doi: 10.1109/IPEC.2010.5542012.
9. T. D. Nguyen and G. Foo, “Sensorless control of a dual-airgap axial flux permanent magnet machine for flywheel energy storage system,” IET Electr. Power Appl., vol. 7, no. 2, pp. 140–149, 2013, doi: 10.1049/iet-epa.2012.0048.
10. D. Won, W. Kim, D. Shin, and C. C. Chung, “High-Gain Disturbance Observer-Based Backstepping Control With Output Tracking Error Constraint for Electro-Hydraulic Systems,” no. m, pp. 1–9, 2014.
11. Q. Dich, Nguyen, and S. Ueno, “Axial position and speed vector control of the inset permanent magnet axial gap type self bearing motor,” IEEE/ASME Int. Conf. Adv. Intell. Mechatronics, AIM, pp. 130–135, 2009, doi: 10.1109/AIM.2009.5230025.
12. Q. D. Nguyen and S. Ueno, “Analysis and control of nonsalient permanent magnet axial gap self-bearing motor,” IEEE Trans. Ind. Electron., vol. 58, no. 7, pp. 2644–2652, 2011, doi: 10.1109/TIE.2010.2076309.
13. H. Khalil and L. Praly, “High-gain observers in nonlinear feedback control,” Int. J. Robust Nonlinear Control, vol. 24, no. 6, pp. 993–1015, 2014, doi: 10.1002/rnc.v24.6.